Int. J. Electrochem. Sci., 16 **(2021)** Article ID: 210822, doi: 10.20964/2021.08.18

International Journal of
ELECTROCHEMICAL
SCIENCE
www.electrochemsci.org

Influence of TiO_2 on Chemical Stability, High Temperature and Electrochemical Properties of Alumina Ceramics based on η-Al_2O_3

Zan Yan[1,2]

[1] College of Chemical Engineering and Modern Materials, Shangluo University, Shangluo, 726000, China
[2] Shaanxi Key Laboratory of Comprehensive Utilization of Tailing resources, Shangluo, 726000, China
E-mail: yanzan2014@163.com, ZanYan@protonmail.com

Received: 8 April 2021/ *Accepted:* 24 May 2021 / *Published:* 30 June 2021

In this paper, the effect of titanium dioxide (TiO_2) on the high temperature performance, chemical stability and electrochemical property of alumina ceramics prepared by nanoη-Al_2O_3 were analyzed. Different contents of TiO_2 (0, 1.5, 2.5 and 3.5 wt%) were added into nanoη-Al_2O_3, and combined with PVA to prepare alumina ceramic samples. The samples were kept at three different sintering temperatures (1450 °C, 1550 °C and 1650 °C) for 2 h, and their properties were measured. The results reveal that the diffusion coefficient and sintering rate of alumina ceramics prepared by nano η-Al_2O_3 showed nonlinear growth as TiO_2 content increased. The results show that the wear resistance, erosion resistance and chemical stability of alumina ceramics prepared by nano η-Al2O3 were very high when the sintering temperature and amount of TiO_2 were 1650°C and 2.5wt%, respectively. The electrochemical property of prepared ceramics was studied by cyclic voltammetry measurements which indicated the enhancement of double-layer capacitive property due to the introducing TiO_2 to Al_2O_3 network.

Keywords: TiO_2; Nanoη-Al_2O_3; High temperature properties; Chemical stability; Sintering rate; Electrochemical property

1. INTRODUCTION

As science and technology advance, material performance is predicted to improve, particularly in the fields of electronic technology, energy, and space technology. Ceramics has evolved into one of the most important materials in human life and modernization, and its concept extends well beyond conventional ceramics. Advanced ceramic material science and production has been a powerful emblem of social and economic progress [1, 2]. Alumina ceramic has the advantages of chemical

stability, high strength, wear resistance and high temperature resistance, and can withstand the harsh working environment that metal materials and polymer materials are not competent for. It has become one of the preferred materials for advanced structural ceramics. It is used in aerospace, fine ceramics, refractories and other fields, and is one of the most widely studied and applied ceramic materials [3-5]. However, the materials in single-phase alumina ceramics are combined by covalent or ionic bonds, and its melting point is as high as 2050 °C, so it is difficult to sinter. At least 1750 °C and sintering for a long time can realize the densification of ceramics, which makes the grain coarsening, intergranular defects and porosity difficult to control, resulting in poor comprehensive properties of ceramics and large energy consumption, which is not conducive to industrial production [6, 7]. Therefore, it is urgent to reduce the sintering temperature, sintering cycle, energy consumption and product performance of alumina ceramics.

To reduce the sintering temperature of alumina ceramics, methods such as improving the fineness and activity of raw materials, special sintering processes, and the addition of sintering additives are commonly used [8]. At present, two methods are mainly used to reduce the sintering temperature of alumina ceramics. One is to reduce the temperature by obtaining monodisperse ultrafine powder with small grain size, large specific surface area and high surface activity. η-Al_2O_3 powder has the characteristics of large specific surface area and high activity, which is widely used in the catalyst support of hydrocracking and hydrodesulfurization [9, 10]. η-Al_2O_3 belongs to the transition state of alumina. During the calcination process, the crystalline phase changes from the transition state to the stable state of α-Al_2O_3. However, because the density of η-Al_2O_3 is less than that of α-Al_2O_3, a large volume shrinkage occurs in the process of atmospheric pressure sintering, resulting in a large porosity and poor compactness. When activated alumina is used in the alumina ceramic industry as a raw material to prepare alumina ceramics, it is typically calcined at high temperatures to convert the activated alumina into alumina of high temperature phase, which not only raises production costs but also limits the performance of alumina ceramics prepared with activated alumina due to alumi's poor size uniformity [11]. Another method is to use appropriate sintering additives (such as TiO_2, MgO, SiO_2, etc.) to improve the diffusion coefficient and reduce the sintering temperature of alumina by forming a solid solution or low-temperature liquid phase with alumina [12, 13]. The densification effect of composite sintering additives is the best, but the types of the second phase will increase, which will affect the content of corundum phase and high-temperature performance [14, 15]; while among the single additives, the best sintering promoter is TiO_2, which belongs to tetragonal system, O^{2-} is hexagonal close packed, Ti^{4+} is in the octahedral gap, located in the 1/2 of the octahedral gap, and the lattice constant of TiO_2 is similar to that of α-Al_2O_3. There are large gaps in both crystal structures, and a limited displacement solid solution can be formed between them [16, 17].

Many studies have been conducted on synthesis of alumina ceramic and its applications in automotive [18], microwave dielectric [19], heat transfer capability of vehicle engine oils [20], and water purification [21]. However, study of the nano η-Al_2O_3 alumina ceramic with the optimal concentration of TiO_2 for improving the ceramic stability and electrochemical properties has not been perfectly studied. Therefore, in this study, nano η-Al_2O_3 alumina ceramic samples were prepared by introducing different amounts of TiO_2 in alumina structures to evaluate the high-temperature performance, chemical stability and electrochemical property of the produced samples.

2. MATERIALS AND METHODS

2.1 Preparation of experimental samples

In order to prepare the nano η-Al_2O_3 powder [6], the 1g $Al(NO_3)_3 \cdot 9H_2O$ (≥98%, Sigma-Aldrich) as precursors were ultrasonically dissolved in deionized (DI) water at 55°C. Then, the solution was mixed and heated under magnetic stirring at 90°C for 5 minutes. After that, the 0.2 g ammonia (32%, Sigma-Aldrich) was ultrasonically added to the solution at room temperature and completely mixed for 10 hours. The obtained pale off-white precipitate was filtered, rinsed, and calcined in an oven at 400 °C for 10 hours.

For preparation of the ceramic samples, 0.1g polyethylene glycol (PEG,>99%, Hubei Honghan Biotech Co., Ltd., China) as dispersant, and the nano TiO_2 powder (99%, Briture Co., Ltd., China) as sintering aid were added into prepared nanoη-Al_2O_3 powder according to the composition ratio of ingredients in Table 1. The powder mixtures were ball milled for 5.5 hours in air at a rate of 180r/min using a planetary ball mill (Tencan, model XQM-2, Changsha, Hunan, China) with anhydrous ethanol (99%, Shijiazhuang Xinlongwei Chemical Co., Ltd., China) as solvent. After drying, 10 wt% polyvinyl alcohol (PVA, >99%, Hebei Yida Cellulose Co., Ltd., China) as binder was added for the granulation process. The resulted granules were passed through 35 mesh sieve, to make a cylindrical sample of φ22×22mm^2 under 100 MPa pressure. After drying at 115 °C for one day, the samples were put into the experimental resistance furnace (SXL-1800C, Xiangtan Instrument Co., Ltd., China) at 560 °C for 1 hour to remove PVA. Subsequently, the heating process was continued to 1450 °C, 1550 °C and 1650 °C for 2 hours for calcination, and cooled to room temperature.

Table 1. The composition ratio of ingredients of samples with different TiO_2 supplemental amounts

Sample	**TiO_2**	**η-Al_2O_3**
S_1	0wt%	100wt%
S_2	1.5wt%	100wt%
S_3	2.5wt%	100wt%
S_4	3.5wt%	100wt%

2.3 Characterization

The samples' high temperature sintering properties were determined using an X-ray diffractometer (XRD, X'Pert Powder, PANalytical B.V., Netherlands), and phase analysis was performed before and after sintering (Cu K1 radiation, step size of 0.02°, 10-90°). The microstructure of the samples was characterized by the IGMA field emission scanning electron microscope (FESEM, LEO SUPRA 55, Carl Zeiss, Oberkochen, Baden-Württemberg, Germany). The acid and alkali resistance of samples were determined according to GB/T 2997-2000. The bulk density and apparent porosity of each group of burned samples were determined using the Archimedes method [8]. The electronic universal testing machine (CMT-6203; MTS System Corporation, China) was used to test

the three-point bending strength of samples. The test interval is 30 mm, and the test rate is 0.5 mm/min. The fracture toughness (K_{IC}) of the specimens was measured by means of crack indentation technique on a material testing machine (Tukon 2100B, Wolpert-Wilson. Instrument, Aachen, Germany) with a load of 49 N [8] which was calculated by Niihara equation [22]:

$$\begin{cases} K_{IC} = 0.089\left(\dfrac{E}{H_V}\right)^{0.4} P \cdot b^{-1} \cdot l^{-0.5} \left(0.25 \le l/b \le 2.50\right) \\ l = d - b \end{cases} \quad (1)$$

Where E is the elastic modulus, P is the indenter load, H_V is the Vickers hardness, d is the half length of the indentation crack, and b is the half diagonal length of the indentation.

Cyclic voltammetry (CV) measurements were performed on Metrohm Autolab instruments (PGSTAT208, Utrecht, Netherlands) using standard three-electrode electrochemical cell containing Pt plate as counter electrode, prepared ceramics as working electrode and Ag/AgCl as reference electrode in 0.1M phosphate buffer solution (PBS) solution pH6 containing 5mM $[Fe(CN)_6]^{3-/4-}$ (99%, Allright GC (Jinan) Biotechnology Ltd., China) as electrolyte. The PBS was prepared from Na_2HPO_4 (99.0%, Zhengzhou Yucai Phosphate Chemical Factory, China).

3. RESULTS AND DISCUSSION

3.1 Analysis of the influence of different amount of TiO_2 on the chemical stability, sintering properties and microstructures of samples

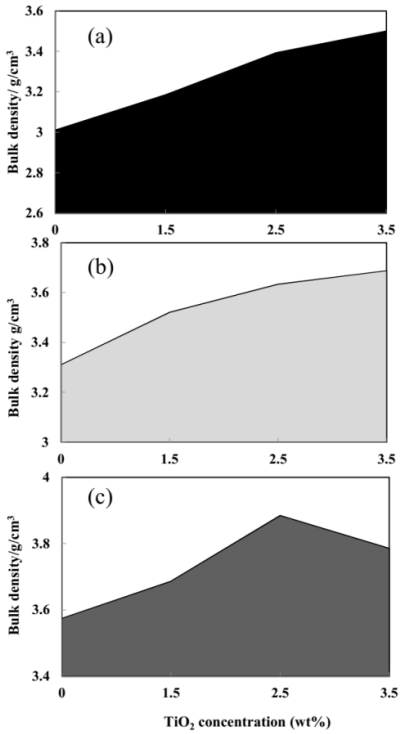

Figure 1. The comparison of the sintered bulk density values of the samples with different amount of TiO_2 at the sintering temperature of (a) 1450°C, (b) 1550°C and (c) 1650°C.

Figure 1 shows the bulk density values of the samples. It can be seen that the bulk density of each sample was gradually increased with the increase of TiO_2 content at different sintering temperatures. When the TiO_2 content was 2.5wt%, the bulk density of each sample was the largest, and the bulk density values were 3.396g/cm^3, 3.634g/cm^3 and 3.885g/cm^3 in turn. It can be related to the solid solubility of TiO_2 in $A1_2O_3$ which is about 0.27% at 1300°C~1700°C. The finer the alumina particles show, the higher the solid solubility [12]. Moreover, the high content of TiO_2 will cause the reverse densification of alumina ceramics. Therefore, when the sintering temperature was 1650°C and the TiO_2 content was 2.5wt%, the bulk density of the sample was the highest.

Table 2 shows the test results from the influence of different TiO_2 amounts on the acid-base resistance of samples sintered at 1650°C which is determined through the acid-base loss rate of samples. As observed, with the increase in TiO_2 concentration, the acid loss rate of the sample varied between 0.85% and 1.78%, and the alkali loss rate varied between 0.87% and 1.75%. When the amount of TiO_2 was 2.5wt%, the acid-base loss rate of the sample was lower, and the acid alkali resistance was better.

Table 2. Test results of acid-base loss rate of sample sintered at 1650°C with different amounts of TiO_2.

Amount of TiO_2	**The acid loss (%)**	**Alkali loss (%)**
0wt%	1.26	1.75
1.5wt%	0.85	1.68
2.5wt%	0.92	0.87
3.5wt%	1.78	1.68

Figure 2 shows the effects of different amounts of TiO_2 on the porosity and flexural strength of the samples which sintered at 1650°C. As seen, the porosity and flexural strength of the sample are changed with the increasing of TiO_2 content. It can be concluded from the analysis of Figure 2 that with the increase of TiO_2 content, the flexural strength of the sample is gradually increased, while the apparent porosity of the sample is gradually decreased, and the chemical stability of the alumina ceramic sample remains relatively stable. The flexural strength of the sample has increased from 55.76 MPa to 82.52 MPa, and the apparent porosity has decreased from 41.59% to 27.22%. When the amount of TiO_2 increases to 3.5wt%, the flexural strength and apparent porosity of the sample change significantly, and the flexural strength of the sample reaches 82.52 MPa, but the apparent porosity is 27.22%, which does not meet the requirement that the apparent porosity of the sample is more than 30%. Therefore, in order to maintain the chemical stability of the flexural strength and apparent porosity of the sample, the amount of TiO_2 should be less than 3.5wt%.

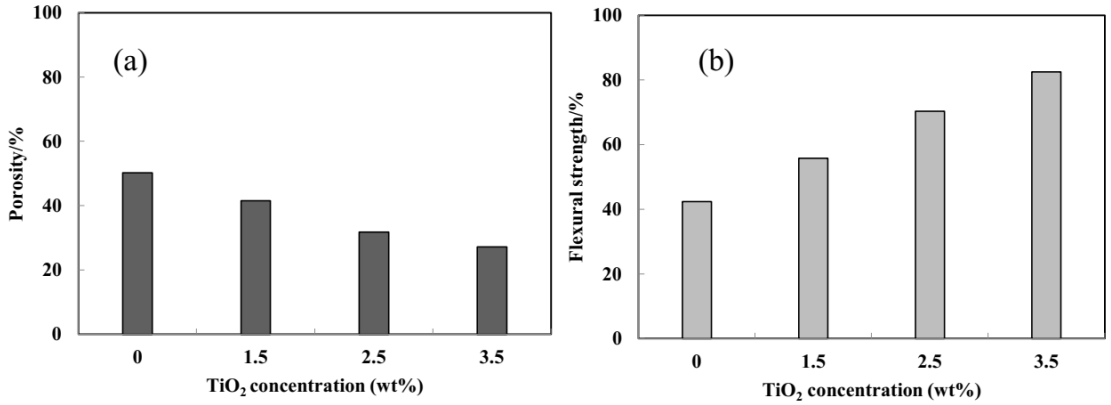

Figure 2. The effect of introducing different amount of TiO_2 on the (a) porosity and (b) the flexural strength of the sample sintered at 1650°C.

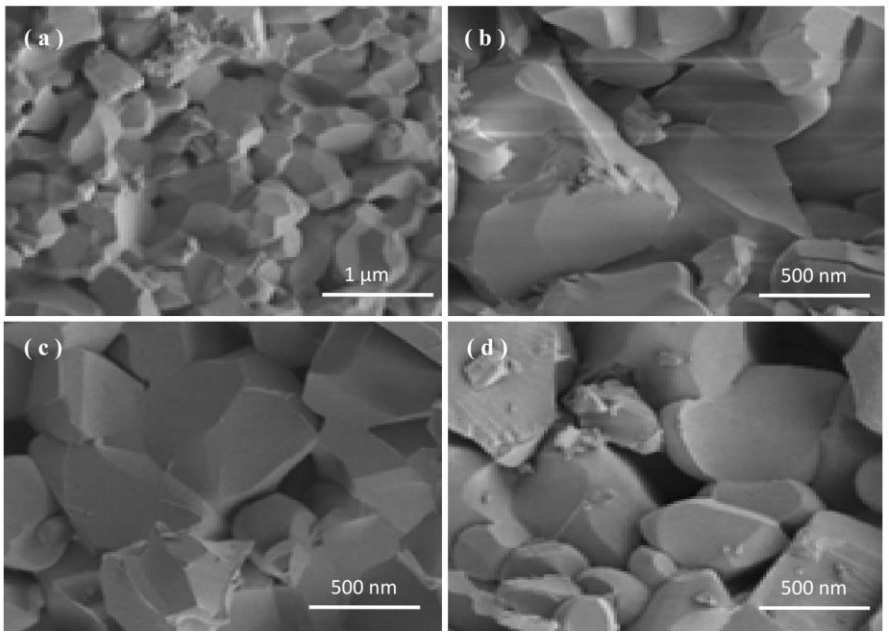

Figure 3. FESEM images of samples at sintered temperature of 1650℃ with (a) 0 wt % TiO_2, (b)1.5 wt % TiO_2, (c) 2.5 wt % TiO_2, and (d) 3.5 wt % TiO_2.

Figure 3 exhibits the FESEM images of alumina ceramic samples prepared by nanoη-Al_2O_3 with different amounts of TiO_2 at a sintering temperature of 1650°C for 2 hours. As observed, from Figure 3a, the grain size distribution of the sample without adding TiO_2 is uniform, but there are more intergranular pores, smaller grain size, and the inner part of the sample is less dense. As shown in Figure 3b, the crystals of the sample grow obviously with the introduction of TiO_2, indicating the great role of TiO_2 in promoting the sintering of the sample. When the amount of TiO_2 is 2.5wt% (Figure 3c), there are less intergranular pores and intergranular bonding. It can be seen from Figure 3d, the number of abnormally grown grains increases when the TiO_2 content is 3.5wt% which results in the increase of intergranular pores and the decrease of density. As a result, the sample densities are reduced to a high

TiO_2 content or to no TiO_2 addition. When the amount of TiO_2 is 2.5wt%, the chemical stability of the sample can be effectively improved.

Figure 4 depicts the XRD patterns of alumina ceramic samples prepared by nanoη-Al_2O_3 with different amounts of TiO_2 at a sintering temperature of 1650°C for 2 hours. It is found that the main crystalline phase of all samples is α-Al_2O_3, except for a small amount of TiO_2 phase, there is no aluminum titanate phase. Aluminum titanate is unstable [23]. A small amount of aluminum titanate is easy to decompose into parent phase oxide when it is cooled to 750°C-1300°C [24], and the decomposition equation is as follows [24]:

$$Al_2TiO_5 \rightarrow \alpha\text{-}Al_2O_3 + TiO_2(\text{rutile}) \qquad (3)$$

The enthalpy of the reaction in equation (3) is negative. When the temperature is lower than 1300°C, it will proceed spontaneously. According to the XRD pattern, the strongest peak of titanium plate type TiO_2 is located at 2θ＝30.832°, the strongest peak of anatase type TiO_2 is located at 2θ＝25.309°, and the strongest peak of rutile type TiO_2 is located at 2θ＝27.434°, while the strongest peak of TiO_2 in Figure 4 is located at 2θ＝27.4513°, indicating that the TiO_2 in the sample is rutile phase.

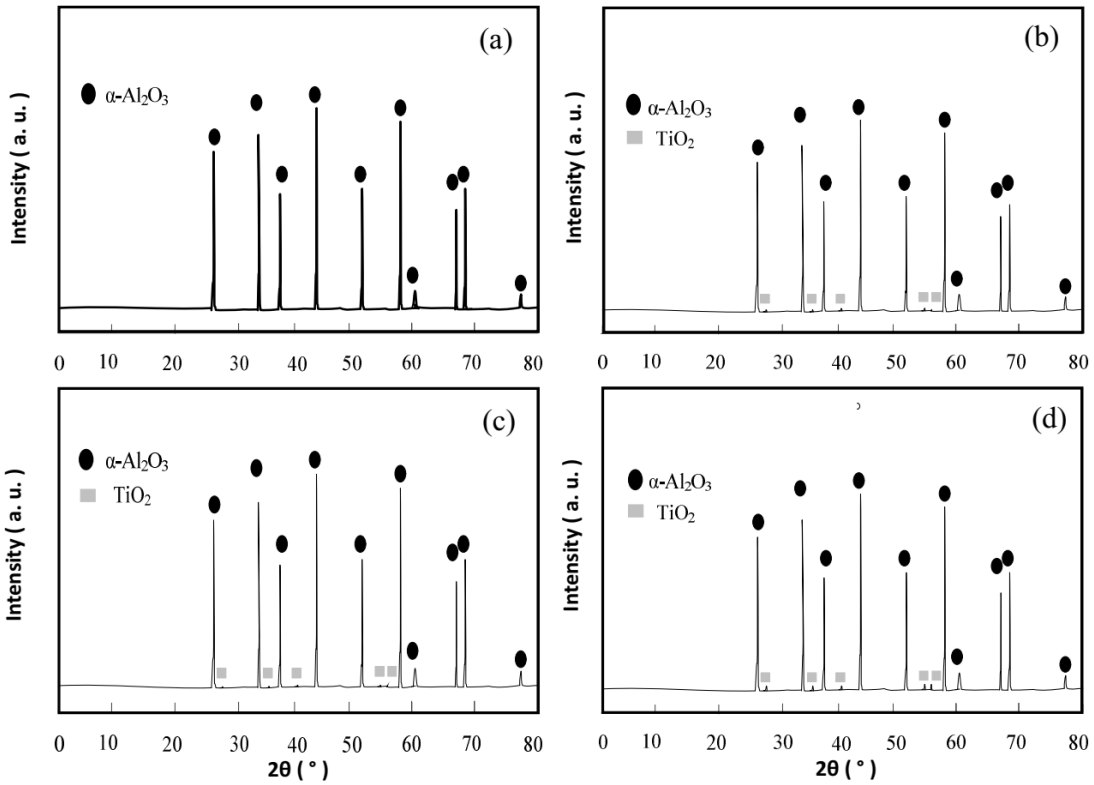

Figure 4. XRD patterns of alumina ceramic samples prepared by nano η-Al_2O_3 sintered temperature of 1650°C for 2 hours with (a) 0 wt % TiO_2, (b) 1.5 wt % TiO_2, (c) 2.5 wt % TiO_2, and (d) 3.5 wt % TiO_2.

In order to determine the crystalline phase in the sample, the unit cell parameters of corundum phase are calculated and compared with the theoretical unit cell parameters of corundum phase. Corundum belongs to the cubic system. The formula for calculating the parameter plane spacing of hexagonal cell in the cubic system is as follows [25, 26]:

$$\frac{1}{d^2} = 4\left(h^2 + k^2 + hk\right)/3a^2 + l^2/c^2 \quad (4)$$

From the associated diffraction peaks, the crystal plane spacing (d) may be calculated. By using the least square method, the equation is changed to $y=kx+B$, $k=1/c^2$, $B=4/3a^2$, $y=1/(h^2+k^2+hk)d^2$, $x=l^2/(h^2+k^2+hk)$. Each diffraction peak has its corresponding (x, y). The slope k and intercept B can be calculated through the straight line from many groups of data points (x, y)according to the principle of least square method, and then the unit cell parameters a and c of corundum phase can be determined. The calculated results are shown in Table 3, where S_t is the theoretical unit cell parameter of corundum.

Table 3. Main crystal phase corundum cell parameters.

Sample	**S_1**	**S_2**	**S_3**	**S_4**	**S_t**
Amount of TiO_2	0 wt%	1.5 wt%	2.5 wt%	3.5 wt%	—
***a* (nm)**	0.47611	0.47613	0.47612	0.47613	0.47610
***c* (nm)**	1.29961	1.29961	1.29963	1.29963	1.29960
$\alpha=\beta$ (°)	90	90	90	90	90
γ (°)	120	120	120	120	120

The actual lattice constants of samples with different amounts of TiO_2 can be obtained by X-ray diffraction. Table 4 shows that the unit cell parameters a and c of samples with different amount of TiO_2 are very close to the theoretical unit cell parameters, and the unit cell parameters of samples with different amount of TiO_2 are almost the same after sintering which indicated to no significant influence of TiO_2 content on the phase composition of samples after sintering.

Table 4. Comparison of actual lattice constants and theoretical lattice constants of Al_2O_3 samples with different quantities addition of TiO_2.

The lattice constant		***a*/nm**	***c*/nm**
The theoretical value [27, 28]		0.0570	0.1297
The actual value	0wt%TiO_2	0.0571	0.1296
	1.5wt%TiO_2	0.0574	0.1299
	2.5wt%TiO_2	0.0578	0.1302
	3.5wt%TiO_2	0.0581	0.1306

It can be seen from Table 4 that the actual lattice constants *a* and *c* of the sample without introducing TiO_2 were very close to the corresponding theoretical lattice constants, which proves that the corundum crystal is well developed, and the sample was not easy to sinter. With the introduction of TiO_2, the actual lattice constants *a* and *c* of the sample indicated an upward trend. With the increase of the amount of TiO_2, the increasing trend of the actual lattice constant was obvious which increases the unit cell defects and makes the sintering easier. It can be demonstrated that increasing TiO2 concentration can enhance sample sintering performance and rate at high temperatures. From the crystallographic point of view, the mechanism of TiO_2 promoting the sintering of Al_2O_3 includes:

(1) The lattice constant of corundum (α-Al_2O_3) was close to that of rutile (TiO_2). Corundum crystal belongs to a hexagonal system that contains oxygen ions which form hexagonal close packing, and aluminum ions which are distributed in two-thirds octahedral space [29]. The rutile crystal belongs to a tetragonal system that contains the oxygen ions which form deformed hexagonal close packing, and titanium ions which are in one-half octahedral space [29]. There were a lot of gaps in both structures, so the diffusion space of ions is large, and they can form displacement solid solution.

(2) The substitution of Ti^{4+} for $A1^{3+}$ is not equivalent, which can be attributed to three Ti^{4+} ions substituted for four Al^{3+} [30]. As a result, a positive ion vacancy is created. The difference in ion radius, crystal structure and electricity price determine that TiO_2 and Al_2O_3 can only form a limited displacement solid solution. This makes the lattice easier to deform and increases the vacancy concentration. The defect equation is as follows [30]:

$$3TiO_2 \xrightarrow{Al_2O_3} 3Ti_{Al}^{\circ} + V_{Al}^{'''} + 6O_O^{\times} \quad (5)$$

Where, Ti_{Al}° represents the substitution of Al^{3+} by Ti^{4+}, the upper right dot represents the residual charge after different valence substitution, and $V_{Al}^{'''}$ is the vacancy of Al^{3+}. The equilibrium constant can be expressed from equation (5) as the following formula:

$$K = \frac{\left[Ti_{Al}^{\circ}\right]^3 \left[V_{Al}^{'''}\right]}{\left[TiO_2\right]^3} \quad (6)$$

The site fractions of defects produced are related by $\frac{1}{3}\left[V_{Al}^{'''}\right] = \left[Ti_{Al}^{\circ}\right]$[30]. Thus, the equilibrium constant can be obtained as equation (7):

$$K = \frac{\frac{1}{27}\left[V_{Al}^{'''}\right]^4}{\left[TiO_2\right]^3} \quad (7)$$

Therefore, equations (8) and (9) can be obtained from equation (7):

$$\left[V_{Al}^{'''}\right]^4 = 27K\left[TiO_2\right]^3 \quad (8)$$

Or

$$\left[V_{Al}^{'''}\right] = (27K)^{\frac{1}{4}}\left[TiO_2\right]^{\frac{3}{4}} \quad (9)$$

The results show that the lattice defect concentration was proportional to the power of 3/4 of TiO_2, and the diffusion coefficient was proportional to the hole concentration. Therefore, the diffusion coefficient and sintering rate of the sample increase nonlinearly with the increase of TiO_2. Accordingly, the high-temperature sintering performance of alumina ceramic samples prepared by nanoη-Al_2O_3 was directly proportional to the amount of TiO_2, but the phase composition of samples with different amount of TiO_2 was not too different after sintering; when the sintering temperature was

1650°C and the amount of TiO_2 was 2.5wt%, the bulk density of alumina ceramic samples prepared by nanoη-Al_2O_3 were the highest, the acid and alkali resistance is best, the apparent porosity and flexural strength can keep stable state, the intergranular bonding was close, the intergranular pores are less, the wear resistance and erosion resistance were higher, and it has strong chemical stability.

3.2. Electrochemical study

Figure 5 displays the CV curves of alumina ceramics prepared by nano η-Al_2O_3 with various concentrations of TiO_2 in 0.1 M PBS solution pH 6 containing 5mM $[Fe(CN)_6]^{3-/4-}$ redox probe solution at a scan rate of 20 mVs^{-1}. As can be seen, the Al_2O_3 sintered temperature of 1650°C with TiO2 has a larger enclosed area of the CV than pure Al_2O_3, indicating that the addition of Ti_{O2} to the Al_2O_3 network improves the double layer capacitive property [31]. It can improve the charge storage value and better electronic storage capability of Al_2O_3 with 2.5 and 3.5 wt% TiO_2 than other prepared alumina ceramics. The TiO_2 tetragonal crystal system contains O^{2-} in hexagonal close packed, Ti^{4+} in octahedral gap which is located in 1/2 of the octahedral gap [32-34]. The lattice constant of TiO_2 is similar to that of η-Al_2O_3. There are large voids in both crystal structures, and a limited displacement solid solution can be formed between them. The replacement process is as follows [24]:

$$3TiO_2 \xrightarrow{Al_2O_3} 3Ti_{Al}^{O} + V_{Al}^{''} + 6O_O \quad (10)$$

In addition, the lowest difference between the anodic and cathodic peak potentials (ΔEp) is observed for Al_2O_3 sintered with 2.5 wt% TiO_2 (0.017 V) which can be attributed to the presence of some imperfect edge stations of the TiO_2 in Al_2O_3 ceramic that increases the number of active sites and has accelerated the electron transfer [35].

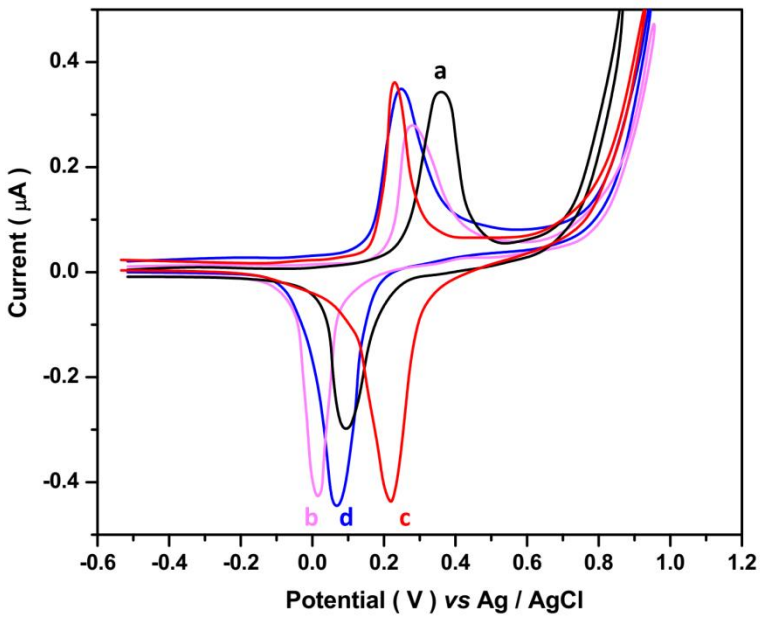

Figure 5. CV curves of alumina ceramics prepared by nano η-Al_2O_3 with (a) 0 wt %, (b) 1.5 wt %, (c) 2.5 wt %, and (d) 3.5 wt % TiO_2in 0.1M PBS solution pH6 containing 5mM $[Fe(CN)_6]^{3-/4-}$ at scan rate of 1mVs^{-1}.

Due to the difference in ionic radius, electrovalence and coordination number, lattice distortion and cation vacancy occur in η-Al_2O_3 after the Ti^{4+} replaces O^{2-}. The activation energy and lattice diffusion coefficient rise, substantially lowering the sintering temperature of alumina ceramics and increasing material density. The larger enclosed area of the CV belongs to theAl_2O_3 sintered with 2.5 and 3.5 wt% TiO_2 due to enhance the conductivity and facilitate electron transport [36, 37].

Moreover, Sopha et al. [38] and Zazpe et al. [39] Suggested that the improvement of the charge storage of Al_2O_3 sintered with TiO_2 can be related to improvement mechanical and chemical stability of composition and presence of TiO_2 preserved their architecture without any noticeable change or damage which is in agreement with SEM results. Karthiket al. [40] also showed that the addition of TiO_2 causes the formation of interfacial layer which acts like a tunnel barrier and helps in formation of capacitance.

4. CONCLUSION

In this paper, the effect of TiO_2 on the high temperature performance and chemical stability of alumina ceramics prepared by nanoη-Al_2O_3 were analyzed. Different contents of TiO_2 (0, 1.5, 2.5 and 3.5 wt%) were added into nanoη-Al_2O_3, and combined with PVA to prepare alumina ceramic samples. The samples were kept at three different sintering temperatures for 2 hours, and the properties of the samples were measured. The results reveal that the diffusion coefficient and sintering rate of alumina ceramics prepared by nano η-Al_2O_3 showed nonlinear growth as TiO_2 content increased. The results show that the wear resistance, erosion resistance and chemical stability of alumina ceramics prepared by nano η-Al_2O_3 were very high when the sintering temperature and amount of TiO_2 were 1650°C and 2.5wt%, respectively. The electrochemical property of prepared ceramics was investigated using CV measurements, which revealed an improvement in double-layer capacitive property due to the addition of TiO_2 to the Al_2O_3 network. Therefore, the prepared by nano η-Al_2O_3 with 2.5wt% TiO_2 in this study can be considered high chemical and mechanical stable ceramic for electrochemical investigation in sensors, capacitors and batteries.

ACKNOWLEDGEMENT
The research was supported by the Open fund project of Shaanxi key laboratory of comprehensive utilization of tailing resources: Study on Roasting-Acid Leaching Quality Improvement of Low Grade Rutile Concentrate in Southern Shaanxi (2017SKY-WK012)

References

1. V. Sabaghi, F. Davar and M.H. Taherian, *Ceramics International*, 45 (2019) 6074.
2. H. Karimi-Maleh, Y. Orooji, A. Ayati, S. Qanbari, B. Tanhaei, F. Karimi, M. Alizadeh, J. Rouhi, L. Fu and M. Sillanpää, *Journal of Molecular Liquids*, 329 (2021) 115062.
3. S. Nazarpour, C. López-Gándara, F. Ramos, C. Zamani, A. Cirera and M. Chaker, *Ceramics International*, 38 (2012) 4813.

4. H. Li, H. Fan, B. Wang, C. Wang, M. Zhang, G. Chen, X. Jiang, N. Zhao, J. Lu and J. Zhang, *Journal of the European Ceramic Society*, 40 (2020) 3072.
5. C. Hu, P. Chen and W. Xiang, *Ceramics International*, 45 (2019) 3263.
6. A.I. Osman, J.K. Abu-Dahrieh, D.W. Rooney, S.A. Halawy, M.A. Mohamed and A. Abdelkader, *Applied Catalysis B: Environmental*, 127 (2012) 307.
7. H. Karimi-Maleh, Y. Orooji, F. Karimi, M. Alizadeh, M. Baghayeri, J. Rouhi, S. Tajik, H. Beitollahi, S. Agarwal and V.K. Gupta, *Biosensors and Bioelectronics*, 184 (2021) 113252.
8. K. Qian, Y. Pan, Z. Hu, X. Chen, Y. Shi, X. Liu, H. Chen, M. Nikl and J. Li, *Journal of the European Ceramic Society*, 40 (2020) 449.
9. M. Dudek and J. Molenda, *MATERIALS SCIENCE-WROCLAW-*, 24 (2006) 45.
10. M. Wang, S. Yuan, B. Lv and H. Yang, *International Journal of Electrochemical Science*, 16 (2021) 210248.
11. B. Gong, P. Wu, J. Yang, X. Peng, H. Deng and G. Yin, *International Journal of Electrochemical Science*, 16 (2021) 21023.
12. H. Wang, H. Ren, T. Yan, Y. Li and W. Zhao, *Scientific reports*, 11 (2021) 1.
13. H. Karimi-Maleh, M.L. Yola, N. Atar, Y. Orooji, F. Karimi, P.S. Kumar, J. Rouhi and M. Baghayeri, *Journal of colloid and interface science*, 592 (2021) 174.
14. Z. Yang, Z. Zhao, J. Yu, Z. Ren, S. Ma and Z. Wang, *Ceramics International*, 45 (2019) 2170.
15. S. Zvonarev, E. Frolov, K.Y. Chesnokov, N. Smirnov, V. Pankov and V. Churkin, *Optical Materials*, 91 (2019) 349.
16. A. Dmitrievskii, A. Zhigachev, D. Zhigacheva and V. Rodaev, *Technical Physics*, 65 (2020) 2016.
17. H. Karimi-Maleh, M. Alizadeh, Y. Orooji, F. Karimi, M. Baghayeri, J. Rouhi, S. Tajik, H. Beitollahi, S. Agarwal and V.K. Gupta, *Industrial & Engineering Chemistry Research*, 60 (2021) 816.
18. P. Srivyas and M. Charoo, *Tribology in Industry*, 40 (2018) 594.
19. J.-M. Wu, S.-S. Liu, M.-Y. Liu, Y. Chen, A.-N. Chen, M. Li, R.-Z. Liu, Y.-S. Shi and C.-H. Li, *Ceramics International*, 44 (2018) 22205.
20. M.K.A. Ali and H. Xianjun, *Powder Technology*, 363 (2020) 48.
21. R. Shang, A. Goulas, C.Y. Tang, X. de Frias Serra, L.C. Rietveld and S.G. Heijman, *Journal of Membrane Science*, 528 (2017) 163.
22. M. Dudek and J. Molenda, *Materials Science Wroclaw*, 24 (2006) 45.
23. M.A. Violini, M.F. Hernández, M.S. Conconi, G. Suárez and N.M. Rendtorff, *Journal of Thermal Analysis and Calorimetry*, 143 (2021) 95.
24. I. Kim and L. Gauckler, *Journal of Ceramic Science and Technology*, 3 (2012) 49.
25. H. Savaloni and R. Savari, *Materials Chemistry and Physics*, 214 (2018) 402.
26. M.F.C. Ladd, R.A. Palmer and R.A. Palmer, *Structure determination by X-ray crystallography*. 1977: Springer.
27. M.-Y. Kuo, C.-L. Chen, C.-Y. Hua, H.-C. Yang and P. Shen, *The Journal of Physical Chemistry B*, 109 (2005) 8693.
28. J.A. Jiménez, I. Padilla, A. López-Delgado, L. Fillali and S. López-Andrés, *International Journal of Applied Ceramic Technology*, 12 (2015) E178.
29. S. Parham, S. Chandren, D.H. Wicaksono, S. Bagherbaigi, S.L. Lee, L.S. Yuan and H. Nur, *RSC advances*, 6 (2016) 8188.
30. C. Pan, P. Shen, W. Huang, S. Hwang, T. Yui and H. Chu, *Journal of the European Ceramic Society*, 26 (2006) 2707.
31. D. Gaboriau, M. Boniface, A. Valero, D. Aldakov, T. Brousse, P. Gentile and S. Sadki, *ACS applied materials & interfaces*, 9 (2017) 13761.
32. F. Wang, P. Chen, X. Li and B. Zhu, *Ceramics International*, 45 (2019)
33. S. Singh and M.N. Tripathi, *Pramana*, 89 (2017) 1.

34. Y. Zhao and X. Zhao, *International Journal of Electrochemical Science*, 16 (2021) 210441.
35. M. Nazari, S. Kashanian, P. Moradipour and N. Maleki, *Journal of Electroanalytical Chemistry*, 812 (2018) 122.
36. L.G. Beka, X. Bu, X. Li, X. Wang, C. Han and W. Liu, *RSC advances*, 9 (2019) 36123.
37. J. Bi and X. Cao, *International Journal of Electrochemical Science*, 16 (2021) 210340.
38. H. Sopha, G.D. Salian, R. Zazpe, J. Prikryl, L. Hromadko, T. Djenizian and J.M. Macak, *ACS omega*, 2 (2017) 2749.
39. R. Zazpe, J. Prikryl, V. Gärtnerova, K. Nechvilova, L. Benes, L. Strizik, A. Jäger, M. Bosund, H. Sopha and J.M. Macak, *Langmuir*, 33 (2017) 3208.
40. R. Karthik, D. Kannadassan, M.S. Baghini and P. Mallick, *Journal of nanoscience and nanotechnology*, 13 (2013) 6894.